

PHYSICAL SIMULATION EXPERIMENTS OF MOMENTUM TRANSPORT ASSOCIATED WITH THE EVOLUTION OF ADVECTING VORTICAL MOTIONS

John R. Elsnab¹

Department of Mechanical Engineering
University of Melbourne¹
Building 170, Level 4, Grattan Street
Parkville, Victoria 3010, Australia
john.elsnab@unimelb.edu.au

Joseph C. Klewicki^{1,2}

Department of Mechanical Engineering
University of New Hampshire²
Kingsbury Hall, W101, 33 Academic Way
Durham, New Hampshire 03824, USA
klewicki@unimelb.edu.au

ABSTRACT

We report on experiments investigating velocity-vorticity interactions that underlie the mechanisms of turbulent inertia associated with advecting regions of concentrated vorticity. To isolate mechanisms and expose the full scope of possible interactions, unsteady laminar flow experiments are conducted. These experiments mimic instantaneous flow field interactions known to exist in turbulent wall-flows. Experiments are conducted in a large water tank. These studied vortex ring interactions with wall effects, a Stokes layer, and imposed advection velocity. Purely advective perturbations to the ring do not introduce any asymmetries whereas interactions with a shear-layer and rings directed towards a wall at a slight angle introduce asymmetries. Shear-layer interactions cause significant asymmetries. This induces a source or sink of momentum in the ring depending upon the sign of spanwise vorticity in the shear-layer.

INTRODUCTION

Time averaging the differential form of Newton's Second Law for turbulent fluid flow introduces an additional unknown term that physically represents the net effect of turbulent inertia. Often researchers investigate the so-called Reynolds stress, but it is the gradient of that appears in time averaged form of Newton's Second Law. Ultimately, this inertial effect is responsible for the establishment of the mean distribution of momentum, its understanding is, therefore, essential to prediction and control.

Herein, we report on experiments investigating velocity-vorticity interactions that underlie the mechanisms of turbulent inertia associated with advecting regions of both concentrated and distributed vortic-

ity. To isolate mechanisms and expose the full scope of possible interactions, unsteady laminar flow experiments using vortex rings are conducted. Previous investigations have studied vortex ring interactions with angled/normal walls and a shear-layer adjacent to a wall (Chu & Falco, 1988; Couch & Krueger, 2011; Lim, 1989; Lim *et al.*, 2008). One motivation behind investigating vortex rings interacting with surfaces and other flows stems from observed similarities to the spatially compact coherent motions in boundary layer flows. It is thought that by understanding vortex ring interactions, insight can be gained in respect to the generic mechanisms in wall-bounded turbulent flows.

Methods and Procedures Experimental Facility

Vortex rings are generated using a 127 mm piston-cylinder device and a 34.8 mm seamless stainless steel tube that is 800 mm long. The cylinder and SS tube are connected using flexible 38.1 mm tubing. The piston-cylinder motion is precisely controlled using LabView and a stepper motor. A vortex ring is produced at the exit of the tube by converting rotational motion from the stepper motor to translation using a 12.7 mm threaded rod with pitch of 2.11 mm/rev. The outer contour at the exit plane of the tube is machined to form a wedge with tip angle of 10° and length of 6 mm. The vortex ring apparatus (VRA) is allowed to translate on 25.4 mm diameter rails. Translational velocity and displacement of the VRA are controlled using LabView and a stepper motor, which drive a timing belt system that is attached to the VRA. A Stokes layer, also referred to as the Rayleigh problem, i.e., a time developing shear-layer, is generated using a conveyor belt that is 305 mm wide and 1.83 m long which rides

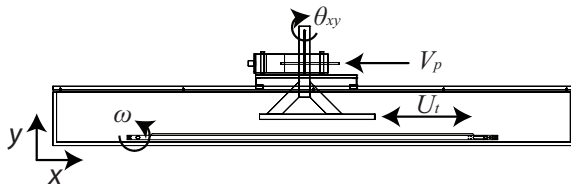


Figure 1. Experimental facility used for the experiments. Note that the servo/stepper motors, timing belts, and flexible tubing are not shown.

on a nominally flat acrylic plate. The conveyor belt is driven by a servo motor and timing belt system. Trapezoidal velocity versus time profiles are implemented in LabView with an impulse configuration, i.e., acceleration time is much less than the overall time interval, T . Since the acceleration time of the shear-layer is $\ll 1$ second, the belt can be considered impulsively started. As time increases, a laminar Stokes layer builds up on the belt that redistributes the spanwise vorticity, which is generated during start up of the conveyor belt. Note that even if one does not consider the belt impulsively started, the amount of vorticity in the layer, i.e., its circulation, is equivalent. Due to unequal time intervals for the vortex ring generation and translation, the timing is set so that the end of the constant velocity region of each respective velocity curve coincide and the conveyor belt continues to move until the vortex ring passes through the field of view. Also note that the Stokes layer thickness scales with \sqrt{t} . Thus, the layer thickness is essentially constant as the ring advects through the field of view since the total image acquisition time is less than 4 seconds. Rotation of the vortex generator tube in the $x-y$ plane, θ_{xy} , is accomplished using a precision rotation stage and is verified using a precision digital level. The vortex generator and conveyor belt are used in a large water tank with width of 1.08 m, length of 3.6 m and height of 0.37 m. A schematic of the apparatus is presented in Figure 1.

Vortex rings are formed using a stroke length, L/D of 1.96, where L is the fluid displacement in the tube and D is the SS tube diameter, at a Reynolds number based upon average slug velocity, $\bar{V}_s = 1/T \int v_s(t) dt$ and tube diameter of 2800. Gharib *et al.* (1998) identified the ratio $L/D = \bar{V}_s T/D$ with the formation time. The translation velocity, U_t , ranged from ± 2.37 cm/sec, which resulted in a perturbation velocity, U_t/U_{cl} , of approximately $\pm 20\%$, where U_{cl} is the centerline velocity obtained by spatial averaging in the streamwise direction centred over $0.1D$ along the x -axis ring centerline. The moving belt velocity ranged from ± 14.3 cm/sec. By rotating the conveyor belt in opposite directions, both same-sign and opposite-sign spanwise vorticity interactions can be investigated.

Experimental Methods

Digital particle imaging velocimetry data are obtained at the wall-normal plane of symmetry ($x-y$ plane). A dual pulse Nd:YAG laser operating at 532 nm is used as the light source. Pulse generators are used to synchronize the laser Q-switch timing to a CCD camera with resolution 4072×2720 pixel². The water tank is seeded with hollow glass sphere parti-

cles, nominally 15 microns in diameter. The time delay between image capture ranges from 3 to 4 ms so that the bulk displacement of the vortex ring ranges from 8 to 10 pixels. Image pairs are captured at a rate of 2 Hz. Timing between image acquisition, shear-layer start-up, vortex ring generation, and apparatus translation is accomplished using the output signal from the pulse generator to trigger LabView. Since this timing method is software based, the accuracy is limited to 0.001 s.

Data Reduction

A multi-pass, multi-grid, cross-correlation method is utilized to determine the particle displacements with a base interrogation window size of 32×32 pixel², which is subsequently divided into four 16×16 pixel² windows. A window shift of 8 pixels (50% overlap) is also utilized in the second pass. The particle diameters ranged from 2 to 3 pixels, which results in an RMS uncertainty of $3.7 - 4.3 \times 10^{-4}$ cm (Raffel *et al.*, 1998). The field of view is $5.6D \times 3.8D$ and starts $2/3D$ from the stopping point of the tube exit. The wall-normal distance from the belt to the center of the tube ranged from $1.5 - 2.5D$. Velocity vector spatial resolution is $0.011D$ for both the streamwise and wall-normal directions. The uncertainty in velocity is less 1% after averaging the instantaneous vector fields over 50 trials. The instantaneous vector fields are phase and conditional averaged on the location of the maximum spanwise vorticity. The kinematic Reynolds stress, UV , is obtained by taking the product of the streamwise velocity, U with the wall-normal component, V . The spanwise vorticity, ω_z , is obtained by differentiating the velocity field using a least-squares method (Foucaut & Stanislas, 2002). The circulation, ζ , on the upper and lower half of the ring is obtained by Stokes theorem, $\equiv \oint_C \mathbf{u} \cdot d\mathbf{l} = \int_A \omega_z dA$, using a two-dimensional version of the trapezoidal rule. The gradient of the Reynolds stress is related to the difference of velocity-vorticity products and streamwise gradient of specific kinetic energy by the following exact relationship

$$\frac{\partial UV}{\partial y} + \frac{\partial UW}{\partial z} = \overline{\omega_y W} - \overline{\omega_z V} + \frac{1}{2} \frac{\partial}{\partial x} (V^2 + W^2 - U^2), \quad (1)$$

where W is the spanwise velocity and ω_y is the wall-normal vorticity (Hinze, 1975). Within the wall-normal plane of symmetry, W and $\partial()/\partial z$ are equal to zero. The first two terms on the RHS of equation 1 may be thought of as the "active" rotational component of the motion, and the last term as the irrotational "inactive" component of the motion (Townsend, 1961).

Results and Discussion

A persistent challenge associated with the study of turbulence relates to determining how and why ensembles of instantaneous motions underlie the observed behaviors of the time averaged flow. As discussed by Smith *et al.* (1991), it is important to distinguish between events that make a lasting and unique signature to the time average representation of the

August 28 - 30, 2013 Poitiers, France

Table 1. Experimental parameters and symbols for the Stokes Layer where δ^* is the displacement thickness, sl is the shear-layer, and vr is the vortex ring.

Re_{δ^*}	δ^*/D	$ \zeta_{sl}/\zeta_{vr} $	Symbol
223	0.19	0.21	\triangle
311	0.13	0.44	\triangleright
360	0.07	0.88	\triangleleft
400	0.11	0.66	\circ
443	0.18	0.44	\square

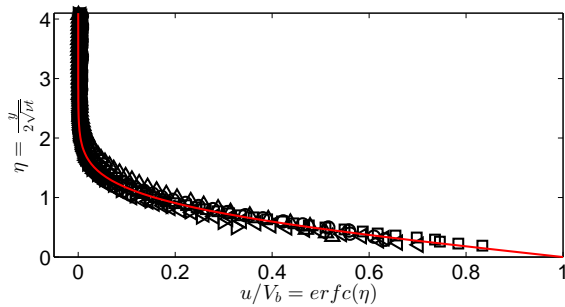


Figure 2. Comparison between the experimental shear-layer results and the analytical solution. Description: Symbols, see Table 1 and red line, analytical solution.

flow, and not events that simply make instantaneous contributions. Specifically, it is easily reasoned that the family of motions of interest contain geometric, kinematic or dynamic asymmetries. With that, a first step is to establish what specific perturbations cause the persistent asymmetry of the vortex ring motion. Since the gradient of the Reynolds stress is the dynamical quantity that appears in the Navier-Stokes equations, it is thought that this term will provide the necessary insight to deduce whether the given kind of perturbation does or does not make a lasting and unique signature to the mean dynamics.

The Stokes layer is generated to explore shear-layer interactions with the ring. Experimental results are shown in Figure 2, and the experimental parameters are summarized in Table 1. As indicated, these profiles of Figure 2 show very good agreement with the analytical solution.

Contours of $\partial\overline{UV}/\partial y$ and $\omega_{z,vr}$ for shear-layer interactions and purely advective perturbations are shown in Figure 3. Early x/D contours are substantially modified by the perturbations in terms of magnitude but not spatial distribution. As x/D increases, certain interactions cause the ring to lose symmetry, e.g., shear-layer interactions and angle perturbations influenced by the wall. This is clearly evident for the same-sign vorticity interaction since the poles in $\partial\overline{UV}/\partial y$ for spatial quadrants 3 and 4 are rotated clockwise in comparison to the early x/D contours, and this rotation is greater than in quadrants 1 and 2. The CW rotation of the ring is clearly shown in the $\omega_{z,vr}$ contours plots

for the the shear-layer interaction. For opposite-sign vorticity interactions, the ring tilt is CCW. In contrast, simply introducing a purely advective perturbation to the ring, regardless of the direction, does not introduce a significant asymmetry in $\partial\overline{UV}/\partial y$, but does cause a slight CW rotation in $\omega_{z,vr}$ due to a wall influence. Similar trends also exist for the angled wall interaction, although they are more subtle, when influenced by the wall, i.e., $y/D < 0.5$ and are more prevalent with increasing θ_{xy} .

Interestingly, these changes to the ring characteristics occur without significant alteration to the rings vorticity field for both positive and negative $\omega_{z,sl}$ interactions (the percent difference between circulation of the bottom and top lobes remains within 7%), but does significantly alter it for the $-\omega_{z,sl}$ $Re_{\delta^*} = 443$ scenario since the maximum difference increases to 20%. The vortex ring for this scenario is influenced more than in the other $-\omega_{z,sl}$ cases due to interaction with a thicker shear-layer. The changes in the overall circulation balance are not noticeable until $x/D \gtrsim 3$.

The trajectory of the vortex cores, i.e., locations of the minimum and maximum $\omega_{z,vr}$, is shown in Figure 5 for angled and shear-layer perturbations. Purely advective perturbations do not alter the trajectory of the vortex cores in comparison to the baseline case for $y/D = 2.5$, where the baseline case refers to an unperturbed ring. The baseline case trajectory, shown in Figure 5 for $y/D = 1.5$, bends towards the wall, which is attributed to a subtle wall effect. Rotating the VRA by 1° and 3° in the clockwise direction causes a nonlinear modification to the trajectory. That is, the trajectory is only mildly altered until the ring starts to further feel the presence of the wall. This alteration increases with increasing θ_{xy} , but does not seem effected by whether the induced advection velocity is in $\pm x$ -direction. The vortex ring is drawn away the wall for opposite-sign vorticity interactions, and towards the wall for same-sign interactions. This apparent lift force is attributed to the alteration of the circulation in the bottom lobe of the ring, and the nearly constant circulation on the top lobe. The circulation of the bottom and top lobes is presented in Figure 6. For same-sign interactions, the ring circulation of the bottom lobe increases, and thus is driven towards the wall. Note that the opposite trend exists for opposite-sign vorticity interactions.

In turbulent wall flows, the gradient of the Reynolds stress ($-\overline{uv}$) acts as a net source or sink of mean momentum depending upon whether $y < y_m$ or $y > y_m$, where y_m is the position where the Reynolds stress is maximum (Klewicki *et al.*, 2007). Mathis *et al.* (2009) also report that in the boundary layer the position where the large-scale modulation effect on the near-wall flow also scales with this transition from mean momentum source to mean momentum sink. Thus, this zero crossing also potentially implies a source/sink behaviour depending upon the sign of the modulation, e.g., positive modulation corresponds to a source and vice-versa.

We now explore properties affecting the overall symmetry of $\partial\overline{UV}/\partial y$ and the overall skewness of the ring motion. Integrating $\partial\overline{UV}/\partial y$ over the vortex ring allows for global comparison to be made on the effects of the perturbation. Since no noticeable asymmetry exists for a purely advective perturbation,

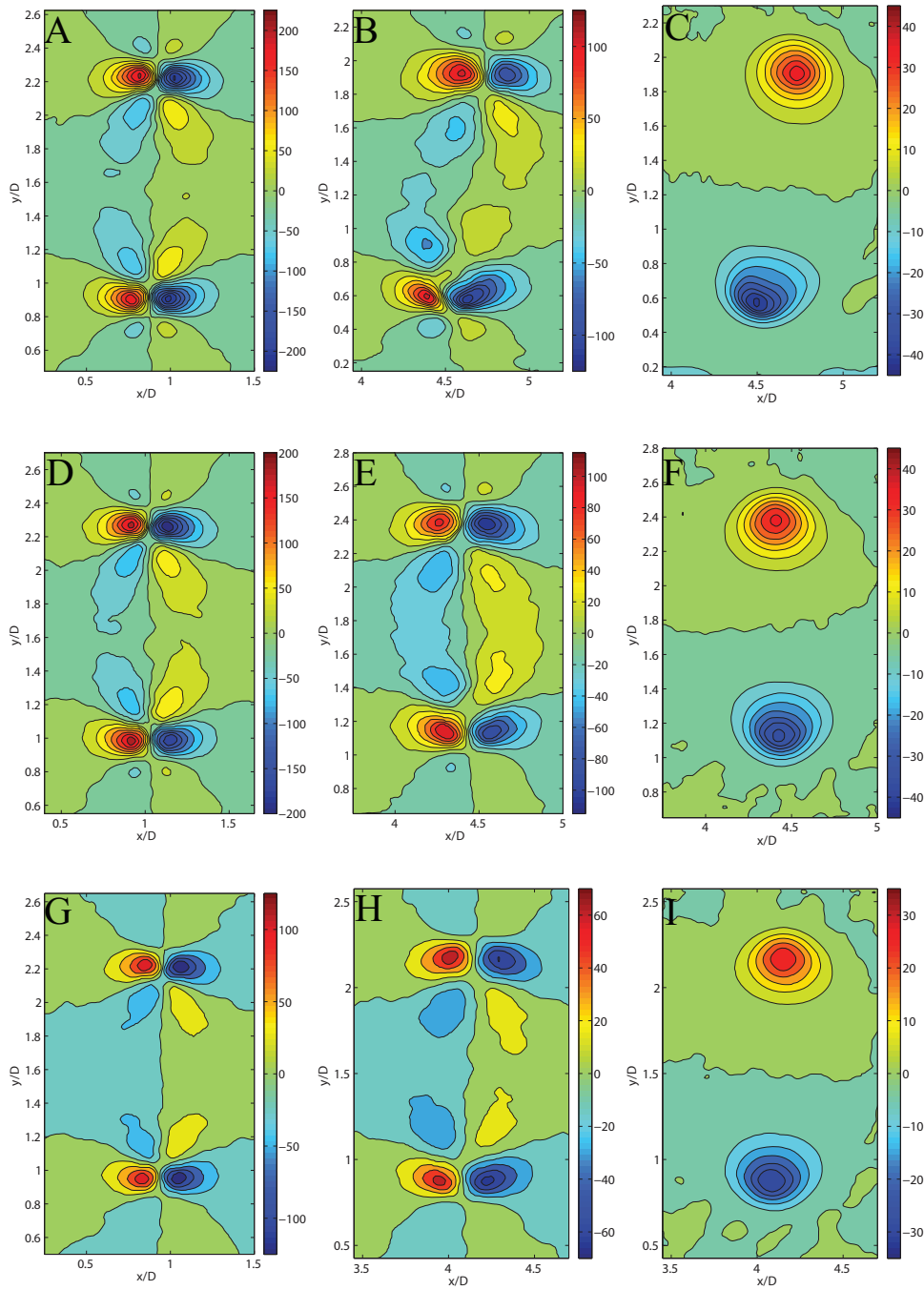


Figure 3. Contours of $\partial \overline{UV} / \partial y$ [cm^2/s] and $\omega_{z,sl}$ [$1/\text{s}$] for $[Re_{\delta^*}, \theta_{xy}, U_t/U_{cl}] =$: Figures A-C, $-\omega_{z,sl}$, [443, 0, 0]; Figures D-F, $\omega_{z,sl}$, [443, 0, 0]; and Figures G-I, [0, 0, -17%].

the integral balance allows for a noise threshold to be established. This noise threshold is required due to the inherent sensitivity in integrating a differential quantity, and is determined to be ± 0.01 [cm^2/s]. Shear layer interactions with positive $\omega_{z,sl}$ indicate that a net drag ($\partial \overline{UV} / \partial y > 0$) is induced on the ring if $Re_{\delta^*} > 300$, albeit with some scatter in the data for $300 < Re_{\delta^*} < 350$. For $-\omega_{z,sl}$ interactions, a source of momentum ($\partial \overline{UV} / \partial y < 0$) is induced on the ring for $Re_{\delta^*} > 300$. However, for the angled cases (including an induced advection velocity) the integral balance is within the noise threshold. This is potentially due to a y/D affect, i.e., the ring does not get close enough to the wall to leave a lasting signature. Other than

Re_{δ^*} , it is not clear what parameter, e.g., y/δ^* or ζ_{or}/ζ_{sl} , dictates the magnitude of the augmentation or attenuation where $\zeta_{sl} = V_b D$ and V_b is the velocity of the belt. The magnitude of the source/sink behavior is greater for the $\omega_{z,sl}$ interaction in comparison to the $-\omega_{z,sl}$ interaction. This is interesting since the change in circulation for the $\omega_{z,sl}$ interaction is approximately the same as $-\omega_{z,sl}$ interactions except for $Re_{\delta^*} = 443$. The results, however, seem consistent with what one would expect since the circulation is responsible for the momentum impulse of the ring.

In the context of concentrated regions of vorticity, a critical question relates to whether the local velocity field (momentum field per unit mass) is experiencing

a net drag or impulse owing to its interaction with the vorticity field (Klewicki *et al.*, 2007). For idealized vortices these interactions are precisely described in terms of a “drift velocity” between the vortex and the surrounding velocity field (Eyink, 2008). This effect produces a Magnus-type force that can be positive or negative depending on the details of the interaction. The drift velocity is given as

$$\Delta u_i = \epsilon_{ijk} \omega_j \frac{g_k}{\omega_1 \omega_1'} \quad (2)$$

where g_k is the nonpotential viscous force given as $-v\epsilon_{klm}\partial/\partial x_l \omega_m$ and v is the kinematic viscosity. Equation 2 simplifies to the following components: $\Delta u_x = -v/\omega_z \partial \omega_z / \partial x$ and $\Delta u_y = -v/\omega_z \partial \omega_z / \partial y$. Since the vortex ring is travelling in the streamwise direction, it is expected that there will be a natural asymmetry in Δu_x and U that can be quantified using the skewness, S . The skewness in Δu_y and V should be zero if the ring remains symmetric. In general, the evolution of the skewness in Δu_x is increasingly positive with x/D , but subsequently decreases to approximately its initial value, although the data are scattered due to the difficulty in calculating the drift velocity. As a surrogate for the drift velocity, we also look at the skewness of the velocity distribution, as integrated over the ring. This measure has apparent connection to the aforementioned modulation phenomena (Mathis *et al.*, 2009), as the skewness of a profile in the boundary layer closely resembles the modulation function. The skewness in U , which is presented in Figure 7, becomes increasingly positive for opposite-sign ω_z interactions and decreases for same-sign interactions. The skewness for the baseline case increases due to the presence of the wall. If y/D is increased to 2.5, $S(U)$ and $S(V)$ are essentially constant at 0.5 and approximately 0, respectively. The skewness in V , which is presented in Figure 8, generally increases for same-sign vorticity interactions and decreases for opposite-sign vorticity interactions. The presence of the wall forces $S(V)$ to increase since V is decreasing. Note that the magnitude of S is relative to the area it is calculated from, but the trend is robust. It is not entirely clear at this point how the asymmetry effects the evolution of the drift velocity or whether the perturbed vortex motion results in a net (integral sense) augmentation or attenuation of the surrounding momentum field.

Conclusions

Vortex rings subjected to an imposed advection velocity, induced rotation towards a wall, and shear-layer interactions have been experimentally investigated. Contours of the wall-normal Reynolds stress gradient are significantly effected by the perturbation in both magnitude and spatial distribution. Purely advective perturbations to the ring do not introduce any appreciable asymmetries whereas, interactions between a wallward moving ring and a shear-layer introduce significant asymmetries to the ring. These interactions induce a source or sink of momentum depending upon the sign of spanwise vorticity in the shear-layer. A modification of the trajectory alone is

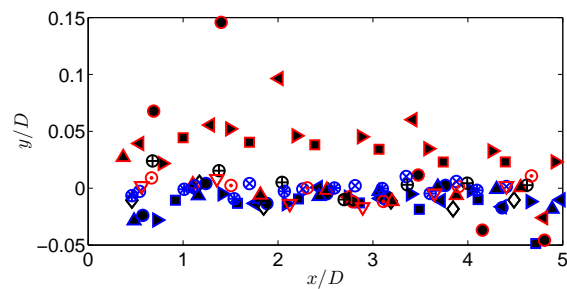


Figure 4. Integral balance of $\partial \overline{UV} / \partial y$. Description: Filled blue marker edge symbols, $-\omega_{z,sl}$, filled red marker edge symbols, $\omega_{z,sl}$, see Table 1 for experimental parameters; $[Re_\delta, \theta_{xy}, U_t/U_{cl}] =$: \diamond , $[0, 0, 0]$; \oplus , $[0, 3^\circ, 0]$; \otimes , $[0, 3^\circ, -17\%]$; \odot , $[0, 3^\circ, 13\%]$; \ominus , $[0, 1^\circ, -17\%]$; and ∇ , $[0, 1^\circ, 13\%]$.

not sufficient to make a significant contribution to the net momentum by the ring. The present results suggest that there is much to be gained by understanding how the Reynolds stress gradient arises, and is modified by introducing specific perturbations. This has potential regarding flow prediction and control applications.

Recent findings by Klewicki (2013) support the interpretation by Tennekes & Lumley (1972) that in the boundary layer the region of positive $\partial \overline{uv} / \partial y$ is where the vorticity stretching term ($w\omega_y$) is dominant, while the region of negative $\partial \overline{uv} / \partial y$ is where the vorticity transport term ($v\omega_z$) is dominant. Therefore, either positive or negative purely advective perturbations do not induce a source or sink on the local momentum field since the integral of the Reynolds stress gradient is approximately zero. However, perturbations that introduce a significant asymmetry can induce a source or sink of momentum since the integral over all of the $\partial \overline{UV} / \partial y$ contours is slightly positive or negative depending upon the type of interaction. Of significance in this context is that the inertial force mechanisms represented in equation 1 are solely derived from interactions between the velocity and vorticity fields for streamwise homogenous flows, and thus are not restricted to vortex like motions, but rather only require vorticity bearing motions. A complicating feature for the current investigation is nonzero contribution of the irrotational term. In well-developed boundary layers, the irrotational part is, on average, about three orders of magnitude smaller than the rotational term Klewicki (1989) and identical zero for fully developed channel/pipe flows; however, for the current investigation, the irrotational term is approximately equal to the rotational term.

REFERENCES

- Chu, C.C. & Falco, R.E. 1988 Vortex ring/viscous wall layer interaction model of the turbulence production process near walls. *Exps. Fluids* **6**, 305 – 315.
- Couch, L.D. & Krueger, P.S. 2011 Experimental investigation of vortex rings impinging on inclined surfaces. *Exps. Fluids* **51**, 1123–1138.
- Eyink, G.L. 2008 Turbulent flow in pipes and channels

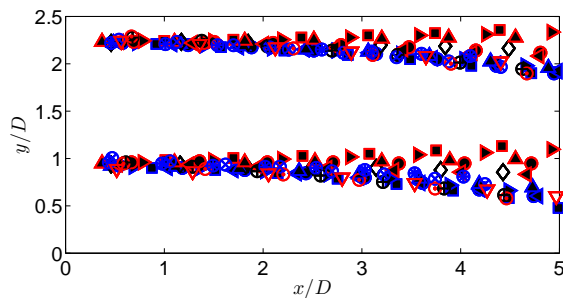


Figure 5. Trajectory of minimum and maximum $\omega_{z, vr}$. See caption for Figure 4 for description of the symbols.

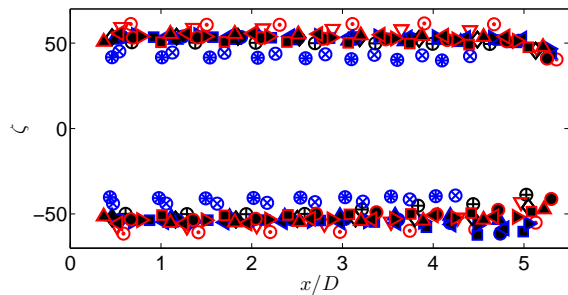


Figure 6. Circulation for the top and bottom lobes of the ring. See caption for Figure 4 for description of the symbols.

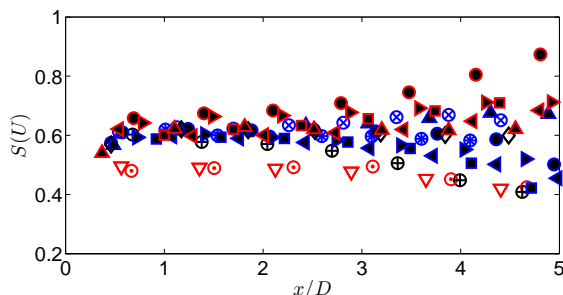


Figure 7. Skewness of U over the vortex ring. See caption for Figure 4 for description of the symbols.

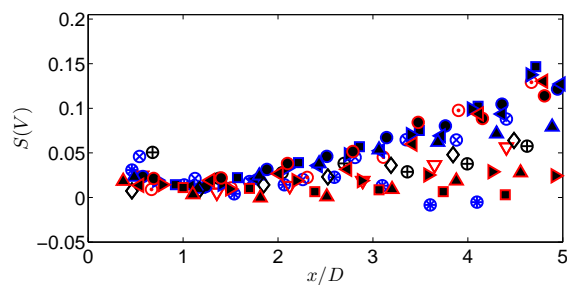


Figure 8. Skewness of V over the vortex ring. See caption for Figure 4 for description of the symbols.

Phil. Trans. R Soc. A **365**, 823 – 839.

Lim, T.T. 1989 An experimental study of a vortex ring interacting with an inclined wall. *Exps. Fluids* **7**, 453–463.

Lim, T.T., Lua, K.B. & Thet, K. 2008 Does Kutta lift exist on a vortex ring in a uniform cross flow. *Phys. Fluids* **20**, 051701–1–4.

Mathis, R., Hutchins, N. & Marusic, I. 2009 Large-scale amplitude modulation of the small-scale structures in turbulent boundary layers. *J. Fluid Mech.* **628**, 311–337.

Raffel, M., Willert, C. & Kompenhans, J. 1998 *Particle image velocimetry: a practical guide*. Springer, Berlin.

Smith, C.R., Walker, J.D.A., Haidari, A.H. & Sobrun, U. 1991 On the dynamics of near-wall turbulence. *Phil. Trans. Phys. Sci. and Eng.* **336**, 131–175.

Tennekes, H. & Lumley, J. 1972 *A First Course in Turbulence*. MIT Press, Cambridge.

Townsend, A.A. 1961 Equilibrium layers and wall turbulence. *J. Fluid Mech.* **11**, 97–120.

as cross-stream “inverse cascades” of vorticity. *Phys. Fluids* **20**, 125101–1–13.

Foucaut, J.M. & Stanislas, M. 2002 Some considerations of the accuracy and frequency response of some derivative filters applied to particle image velocimetry vector fields. *Meas. and Science Tech.* **13**, 1058–1071.

Gharib, M., Rambod, E. & Shariff, K. 1998 A universal time scale for vortex ring formation. *J. Fluid Mech.* **360**, 121–140.

Hinze, J.O. 1975 *Turbulence*, 2nd edn. McGraw-Hill.

Klewicki, J.C. 1989 Velocity-vorticity correlations related to the gradients of the Reynolds stress in parallel turbulent wall flows. *Phys. Fluids A* **1**, 1285–1288.

Klewicki, J.C. 2013 Self-similar mean dynamics in turbulent wall flows. *J. Fluid Mech.* **596–612**, 1285–1288.

Klewicki, J.C., Fife, P., Wei, T. & McMurtry, P. 2007 A physical model of the turbulent boundary layer consonant with mean momentum balance structure.